Acta Mech 229, 1311–1320 (2018)
https://doi.org/10.1007/s00707-017-2041-y

ORIGINAL PAPER

Yang Sun · Xueming Yu · Wenbing Jia · Xianhui Wang · Mabao Liu

The interaction of a mode II crack with an inhomogeneity undergoing a stress-free transformation strain

Received: 30 August 2016 / Published online: 17 November 2017

Abstract In this investigation, general approximate solutions for the stress intensity factor (SIF) and configuration force (CF) are derived, respectively, based on the Eshelby theory for the interaction between an inhomogeneous inclusion of arbitrary shape undergoing a stress-free transformation strain and plane stress mode II crack. For common inclusion shapes, some simplified approximate formulae are also developed. Then, the relationship between the normalized CF and SIF is discussed, as well as the effects of inclusion shape, location, and size on the CF and SIF of a plane stress mode II crack. To give deep insight into the complex three-dimensional interaction between an inclusion undergoing a stress-free transformation strain and a crack, two typical cases of the triaxial stress state are analyzed, and no significant difference occurs among most engineering materials.

1 Introduction

Thin films including inclusions have various applications in the fields such as semiconductors [1], solar cells [2], engine [3] and intelligent coating sensors [4,5], and the interfacial debonding between the matrix and inclusions of the composite film is one of the main failure factors in these applications. An uncontrolled debonding may deteriorate the properties of the device [6]. Subsequently, the penetration/deflection behavior of a crack accessing an inclusion-matrix interface plays a dominant role in the design of a composite thin film [7,8], and this behavior is strongly influenced by the interaction between the crack and the inhomogeneity. On the other hand, the interaction is mainly influenced by the differences of the elastic properties between the inclusion and matrix, the size and shape as well as the distribution in the matrix of the inclusion. Hence, a large number of the investigations has been reported on the crack-inhomogeneity interaction in the past years

Y. Sun · M. Liu (✉)
State Key Laboratory for Strength and Vibration of Mechanical Structures, School of Aerospace, Xi'an Jiaotong University, Xi'an 710049, China
E-mail: mliu@mail.xjtu.edu.cn

X. Yu · W. Jia
Xi'an Satellite Control Center, Xi'an 710043, China

X. Wang
School of Materials Science and Engineering, Xi'an University of Technology, Xi'an 710048, China
E-mail: xhwang693@xaut.edu

Present address:
Y. Sun
State Key Laboratory of Astronautic Dynamics, Xi'an Satellite Control Center, Xi'an 710043, China
E-mail: yang_sun@foxmail.com

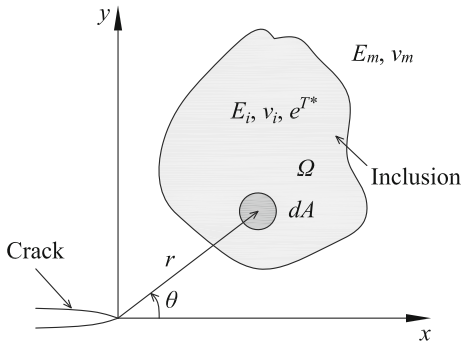

Fig. 1 A plane stress mode II crack interacts with an inclusion of arbitrary shape undergoing a stress-free transformation strain

[9]. Because of its complexity, only a few analytical solutions can be obtained, such as elliptical inclusion [10] and circular inclusion [11].

An inhomogeneous inclusion can be transformed to a homogenous one with an equivalent transformation strain based on the Eshelby theory [12].Thus, the interaction between crack and inclusion can be evaluated from the transformation toughening theory [13] and the configuration force theory [14]. Recently, based on this approach some approximate analytical solutions have been obtained for the interaction of an inclusion of arbitrary shape with mode I and mode II cracks evaluated by stress intensity factors (SIFs) [15–18] and configuration forces (CFs) [19]. However, these solutions neglect the fact that an inhomogeneous inclusion may be subjected to a stress-free transformation strain induced by micro-cracking [20], thermal expansion mismatch, etc., and are limited to the plane strain. In the present work, the interaction between an inclusion of arbitrary shape undergoing a stress-free transformation strain and plane stress mode II crack is investigated.

2 Model and formulation

As shown in Fig. 1, the inclusion undergoes a stress-free transformation strain, $\mathbf{e}^{\mathrm{T}*}$, and simultaneously sustains an applied strain field of the mode II crack tip, $\mathbf{e}^{\mathrm{A}}$. A differential element dA is considered in this work. According to the Eshelby approach [12,21,22], the equivalent transformation strain in dA, $\mathbf{e}^{\mathrm{T}}$, is given by

$$\mathbf{e^T}=[(\mathbf{C_i}-\mathbf{C_m})\mathbf{S}+\mathbf{C_m}]^{-1}[(\mathbf{C_m}-\mathbf{C_i})\mathbf{e^A}+\mathbf{C_i}\mathbf{e^{T*}}] \tag{1}$$

where $\mathbf{S}$ is the Eshelby tensor, dependent solely upon the shape of the inclusion and Poisson's ratio of the matrix material. $\mathbf{C}_{\mathrm{m}}$ and $\mathbf{C}_{\mathrm{i}}$ are the elastic tensors of the matrix and the inclusion material, respectively.

The nonzero components for plane stress condition of $\mathbf{e}^{\mathrm{A}}$ can be expressed as

$$\left.\begin{aligned} e_{11}^{A} &= \frac{K_{\mathrm{II}}}{E_{\mathrm{m}}\sqrt{2\pi r}}\sin\frac{\theta}{2}\left[-2-(1+\nu)\cos\frac{\theta}{2}\cos\frac{3\theta}{2}\right] \\ e_{22}^{A} &= \frac{K_{\mathrm{II}}}{E_{\mathrm{m}}\sqrt{2\pi r}}\sin\frac{\theta}{2}\left[2\nu+(1+\nu)\cos\frac{\theta}{2}\cos\frac{3\theta}{2}\right] \\ e_{12}^{A} &= \frac{K_{\mathrm{II}}}{E_{\mathrm{m}}\sqrt{2\pi r}}(1+\nu)\cos\frac{\theta}{2}\left(1-\sin\frac{\theta}{2}\sin\frac{3\theta}{2}\right) \end{aligned}\right\} \tag{2}$$

where E_m is Young's modulus of the matrix, and K_{II} is the remotely applied mode II stress intensity factor (SIF).

For simplicity, it is assumed that the matrix material and inclusion are isotropic and their Poisson's ratios are the same, denoted by ν. Then

$$\mathbf{C_i}=\alpha\mathbf{C_m} \tag{3}$$

where

$$\alpha = E_{\mathrm{i}}/E_{\mathrm{m}}. \tag{4}$$

E_i is Young's modulus of the inclusion.

Combining Eqs. (1) and (3) gives

$$\begin{aligned}\mathbf{e^T} &= \mathbf{e^{TA}} + \mathbf{e^{Te}} \\ &= (1-\alpha)[(\alpha-1)\mathbf{S}+\mathbf{I}]^{-1}\mathbf{e^A} + \alpha[(\alpha-1)\mathbf{S}+\mathbf{I}]^{-1}\mathbf{e^{T*}}\end{aligned} \tag{5}$$

where $\mathbf{I}$ is the unit tensor.

The Eshelby tensor $\mathbf{S}$ for plane stress can be derived from that for plane strain by replacing ν with $\nu/(1+\nu)$ for a differential element with circular section inside the inclusion [23]. Thus,

$$\mathbf{S} = \frac{1}{8}\begin{bmatrix} 5+\nu & 3\nu-1 & 0 \\ 3\nu-1 & 5+\nu & 0 \\ 0 & 0 & 6-2\nu \end{bmatrix}. \tag{6}$$

Substituting Eqs. (2) and (6) into Eq. (5) yields

$$\left.\begin{aligned} e_{11}^T &= \tfrac{2K_{\mathrm{II}}}{E_{\mathrm{m}}\sqrt{2\pi r}}\left[C_1 - 2C_2\left(1+\cos\tfrac{\theta}{2}\cos\tfrac{3\theta}{2}\right)\right]\sin\tfrac{\theta}{2} \\ &\quad + \tfrac{C_3+C_4}{2}e_{11}^{T*} + \tfrac{C_3-C_4}{2}e_{22}^{T*} \\ e_{22}^T &= \tfrac{2K_{\mathrm{II}}}{E_{\mathrm{m}}\sqrt{2\pi r}}\left[C_1 + 2C_2\left(1+\cos\tfrac{\theta}{2}\cos\tfrac{3\theta}{2}\right)\right]\sin\tfrac{\theta}{2} \\ &\quad + \tfrac{C_3-C_4}{2}e_{11}^{T*} + \tfrac{C_3+C_4}{2}e_{22}^{T*} \\ e_{12}^T &= \tfrac{4K_{\mathrm{II}}}{E_{\mathrm{m}}\sqrt{2\pi r}}C_2\cos\tfrac{\theta}{2}\left(1-\sin\tfrac{\theta}{2}\sin\tfrac{3\theta}{2}\right) + C_5 e_{12}^{T*} \end{aligned}\right\} \tag{7}$$

where

$$\left.\begin{aligned} C_1 &= -\tfrac{(1-\alpha)(1-\nu)}{1+\alpha+\alpha\nu-\nu}, \quad C_2 = \tfrac{(1-\alpha)(1+\nu)}{1+\nu+3\alpha-\alpha\nu} \\ C_3 &= C_5 = \tfrac{4\alpha}{1+\nu+3\alpha-\alpha\nu}, \quad C_4 = \tfrac{2\alpha}{1+\alpha+\alpha\nu-\nu} \end{aligned}\right\}. \tag{8}$$

2.1 Configuration force (CF)

Per unit thickness of the differential element, the reduction in elastic energy is given by [24]

$$\mathrm{d}W = -\sigma_{ij}^A e_{ij}^T \mathrm{d}A \tag{9}$$

where σ_{ij}^A is the stress field of the mode II crack tip, expressed as

$$\left.\begin{aligned} \sigma_{11}^A &= -\tfrac{K_{\mathrm{II}}}{\sqrt{2\pi r}}\sin\tfrac{\theta}{2}\left(2+\cos\tfrac{\theta}{2}\cos\tfrac{3\theta}{2}\right) \\ \sigma_{22}^A &= \tfrac{K_{\mathrm{II}}}{\sqrt{2\pi r}}\sin\tfrac{\theta}{2}\cos\tfrac{\theta}{2}\cos\tfrac{3\theta}{2} \\ \sigma_{12}^A &= \tfrac{K_{\mathrm{II}}}{\sqrt{2\pi r}}\cos\tfrac{\theta}{2}\left(1-\sin\tfrac{\theta}{2}\sin\tfrac{3\theta}{2}\right) \end{aligned}\right\}. \tag{10}$$

Then,

$$\mathrm{d}W = -\left(\frac{K_{\mathrm{II}}^2}{2\pi E_{\mathrm{m}} r} f_I + \frac{K_{\mathrm{II}}}{\sqrt{2\pi r}} f_{\mathrm{II}}\right)\mathrm{d}A \tag{11}$$

where

$$\left.\begin{aligned} f_I &= -4C_1\sin^2\tfrac{\theta}{2} + C_2\left[6\cos^2\theta - 2\cos\theta\cos 2\theta + \tfrac{\sin^2\theta}{2}(3+\cos 3\theta)\right] \\ f_{\mathrm{II}} &= \sin\tfrac{\theta}{2}\left[-C_3\left(e_{11}^{T*}+e_{22}^{T*}\right) + C_4\left(1+\cos\tfrac{\theta}{2}\cos\tfrac{3\theta}{2}\right)\left(e_{22}^{T*}-e_{11}^{T*}\right)\right] \\ &\quad + C_5 e_{12}^{T*}\cos\tfrac{\theta}{2}\left(1-\sin\tfrac{\theta}{2}\sin\tfrac{3\theta}{2}\right) \end{aligned}\right\}. \tag{12}$$

In the absence of body forces, from Eq. (11) the CF can be obtained [25],

$$F_r = \int_\Omega \mathrm{d}F_r = -\int_\Omega \frac{\partial}{\partial r}(\mathrm{d}W) = -\int_\Omega \left(\frac{K_{\mathrm{II}}^2}{2\pi E_{\mathrm{m}} r^2} f_I + \frac{K_{\mathrm{II}}}{2\sqrt{2\pi r^3}} f_{\mathrm{II}} \right) \mathrm{d}A. \tag{13}$$

The total CFs along x and y directions are, respectively, expressed as

$$F_x = \int_\Omega \mathrm{d}F_x = \int_\Omega \mathrm{d}F_r \cos\theta, \tag{14}$$

$$F_y = \int_\Omega \mathrm{d}F_y = \int_\Omega \mathrm{d}F_r \sin\theta. \tag{15}$$

2.2 Stress intensity factor (SIF)

Under plane stress conditions, the change of the crack tip stress intensity factor can be expressed as [16]

$$\mathrm{d}K_{\mathrm{II}}^{\mathrm{tip}} = \frac{E_{\mathrm{m}}}{16\sqrt{2\pi}} r^{-3/2} \varphi(e_{\alpha\beta}^T, \theta) \mathrm{d}A \tag{16}$$

where

$$\begin{aligned} \varphi(e_{\alpha\beta}^T, \theta) = &-\left(5e_{11}^T + 3e_{22}^T\right) \sin\tfrac{3\theta}{2} + 2e_{12}^T \left(3\cos\tfrac{7\theta}{2} + \cos\tfrac{3\theta}{2}\right) \\ &+ 3\left(e_{22}^T - e_{11}^T\right) \sin\tfrac{7\theta}{2} \end{aligned}. \tag{17}$$

Substituting Eqs. (7) and (17) into Eq. (16) and then integrating Eq. (16) over the whole domain Ω, the $K_{\mathrm{II}}^{\mathrm{tip}}/K_{\mathrm{II}}$ can be expressed as

$$\frac{K_{\mathrm{II}}^{\mathrm{tip}}}{K_{\mathrm{II}}} = 1 + \frac{1}{4\pi} \int_\Omega r^{-2} g_I \mathrm{d}A + \frac{E_{\mathrm{m}}}{4\sqrt{2\pi} K_{\mathrm{II}}} \int_\Omega r^{-3/2} g_{\mathrm{II}} \mathrm{d}A \tag{18}$$

where

$$\left.\begin{aligned} g_I &= C_1 \cos 2\theta + \tfrac{9}{4} C_2 \cos 3\theta + C_6 \cos\theta \\ g_{\mathrm{II}} &= -C_3 \left(e_{11}^{T*} + e_{22}^{T*}\right) \sin\tfrac{3\theta}{2} + \tfrac{C_4\left(e_{22}^{T*} - e_{11}^{T*}\right)}{4} \left(\sin\tfrac{3\theta}{2} + 3\sin\tfrac{7\theta}{2}\right) \\ &\quad + \tfrac{C_5 e_{12}^{T*}}{2} \left(\cos\tfrac{3\theta}{2} + 3\cos\tfrac{7\theta}{2}\right) \end{aligned}\right\} \tag{19}$$

and

$$C_6 = \frac{(1-\alpha)\left[11(1+\alpha\nu^2-\nu^2) + 19\alpha - 2\alpha\nu\right]}{4(1+\nu+3\alpha-\alpha\nu)(1+\alpha+\alpha\nu-\nu)}. \tag{20}$$

In addition, the CF and SIF formulae for plane strain are formally identical to Eqs. (13) and (18). However, the constants C_1, C_2, C_3, C_4, C_5 in Eq. (13) and $C_1, C_2, C_3, C_4, C_5, C_6$ in Eq. (18) are different from those of plane strain, in which ν is replaced with $\nu/(1+\nu)$ for plane stress.

3 Simple formulas for special inclusion shapes

To visualize the basic characters of the CF and SIF, some special inclusion shapes are taken as examples:
(i) A small circular inclusion of radius R centered at (r_0, θ). From Eqs. (13) and (18), the CF and SIF can be approximated by

$$F_r = -\left(\frac{R^2 K_{\mathrm{II}}^2}{2E_{\mathrm{m}} r_0^2} f_I + \frac{R^2 K_{\mathrm{II}}}{2} \sqrt{\frac{\pi}{2r_0^3}} f_{\mathrm{II}} \right), \tag{21}$$

$$\frac{K_{\mathrm{II}}^{\mathrm{tip}}}{K_{\mathrm{II}}} = 1 + \frac{R^2}{4r_0^2} g_I + \frac{E_{\mathrm{m}} R^2}{4K_{\mathrm{II}}} \sqrt{\frac{\pi}{2r_0^3}} g_{\mathrm{II}}. \tag{22}$$

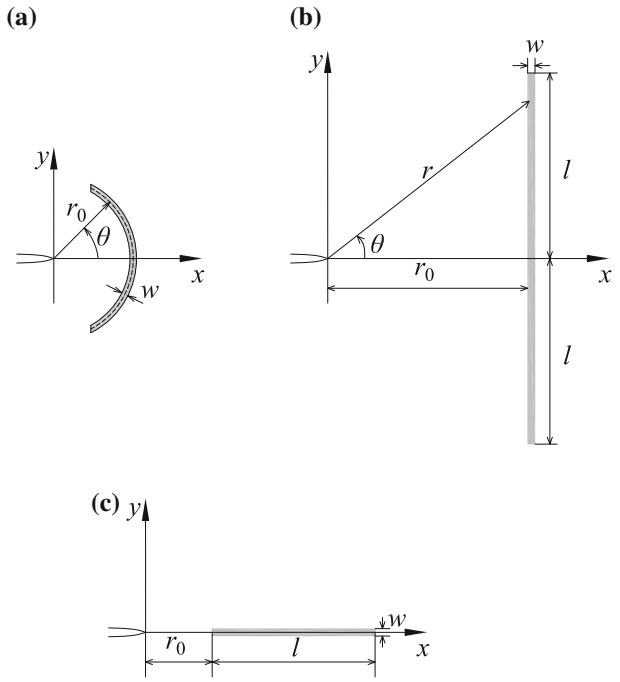

Fig. 2 Mode II crack interacts with some special inclusions: **a** the circular ring-shaped inclusion in the front of a crack tip symmetrically ($r_0 >> w$); **b** the lamellar inclusion perpendicular to the x-axis and centered at $(r_0, 0)(l >> w)$; **c** the lamellar inclusion lies on the x-axis ($l >> w$)

(ii) As shown in Fig. 2a, for a circular ring-shaped inclusion, by use of $\mathrm{d}A \approx w r_0 d\theta$ in Eqs. (13) and (18), respectively, then

$$\begin{aligned} F_r = &-\frac{w K_{\mathrm{II}}^2}{2\pi E_{\mathrm{m}} r_0}\left[-4C_1\left(\theta_0 - \sin\theta_0\right)\right. \\ &\left. + \frac{C_2}{2}\left(15\theta_0 - \frac{9}{2}\sin\theta_0 + \frac{9}{2}\sin 2\theta_0 - \sin 3\theta_0 - \frac{1}{10}\sin 5\theta_0\right)\right] \\ &- \frac{w K_{\mathrm{II}}}{2\sqrt{2\pi r_0}} C_5 e_{12}^{T*}\left(3\sin\frac{\theta_0}{2} + \frac{1}{5}\sin\frac{5\theta_0}{2}\right), \end{aligned} \tag{23}$$

$$\begin{aligned} \frac{K_{\mathrm{II}}^{\mathrm{tip}}}{K_{\mathrm{II}}} = &1 + \frac{w}{4\pi r_0}\left(2C_6\sin\theta_0 + C_1\sin 2\theta_0 + \frac{3}{2}C_2\sin 3\theta_0\right) \\ &+ \frac{E_{\mathrm{m}} w}{4\sqrt{2\pi r_0} K_{\mathrm{II}}} C_5 e_{12}^{T*}\left(\frac{6}{7}\sin\frac{7\theta_0}{2} + \frac{2}{3}\sin\frac{3\theta_0}{2}\right). \end{aligned} \tag{24}$$

(iii) As shown in Fig. 2b, for a lamellar inclusion perpendicular to the x-axis, by use of approximation $\mathrm{d}A \approx w r \mathrm{d}\theta/\cos\theta$ in Eqs. (13) and (18), respectively, then

$$\begin{aligned} F_r &= -\int_{-\theta_0}^{\theta_0}\left(\frac{K_{\mathrm{II}}^2 w}{2\pi E_{\mathrm{m}} r_0} f_I + \frac{K_{\mathrm{II}} w}{2}\sqrt{\frac{1}{2\pi r_0\cos\theta}} f_{\mathrm{II}}\right)\mathrm{d}\theta \\ &= \frac{K_{\mathrm{II}} w}{\sqrt{r_0}}\int_{-\theta_0}^{\theta_0} f_r \mathrm{d}\theta \end{aligned} \tag{25}$$

where $f_r = -K_{\mathrm{II}} f_I/(2\pi E_{\mathrm{m}}\sqrt{r_0}) - f_{\mathrm{II}}\sqrt{1/(2\pi\cos\theta)}/2$ is the distribution forces along the lamellar inclusion (in unit of $K_{\mathrm{II}} w/\sqrt{r_0}$), and $\theta_0 = arctgl/r_0$,

$$\frac{K_{\mathrm{II}}^{\mathrm{tip}}}{K_{\mathrm{II}}} = 1 + \frac{w}{4\pi r_0}\left(2C_6\sin\theta_0 + C_1\sin 2\theta_0 + \frac{3}{2}C_2\sin 3\theta_0\right) + \frac{E_{\mathrm{m}} w}{4\sqrt{2\pi r_0} K_{\mathrm{II}}}\int_{-\theta_0}^{\theta_0}\frac{g_{\mathrm{II}}}{\sqrt{\cos\theta}}\mathrm{d}\theta\,. \tag{26}$$

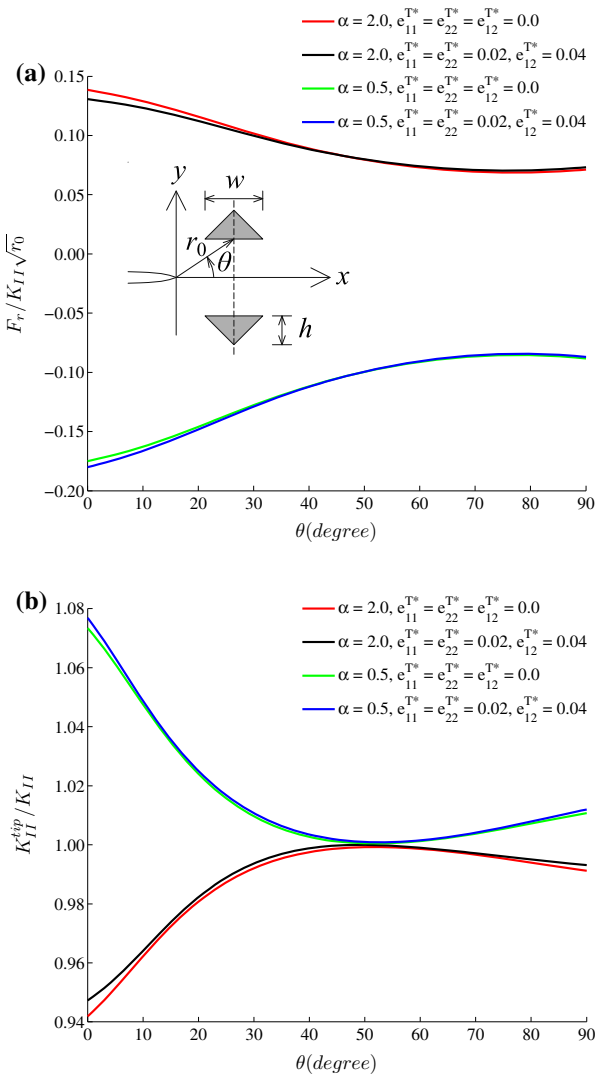

Fig. 3 Normalized CF $F_r/K_{\mathrm{II}}\sqrt{r_0}$ and SIF $K_{\mathrm{II}}^{\mathrm{tip}}/K_{\mathrm{II}}$ as functions of the angle θ for a mode II crack interacting with two isosceles right-angled triangular inclusions of different α and $\mathbf{e}^{T*}$ calculated from Eqs. (13) and (18), respectively, at the fixed $\nu = 0.3$ and $K_{\mathrm{II}}/E_{\mathrm{m}}\sqrt{r_0} = 1$

(iv) As shown in Fig. 2c, for a lamellar inclusion lying on the x-axis, by use of $\mathrm{d}A = wdr$ and $\sin\theta = 0$, $\cos\theta = 1$ in Eqs. (13) and (18), respectively, then

$$F_r = \frac{2wC_2K_{\mathrm{II}}^2}{\pi E_{\mathrm{m}}}\left(\frac{1}{r_0+l}-\frac{1}{r_0}\right)+\frac{wC_5e_{12}^{T*}K_{\mathrm{II}}}{\sqrt{2\pi}}\left(\frac{1}{\sqrt{r_0+l}}-\frac{1}{\sqrt{r_0}}\right), \tag{27}$$

$$\frac{K_{\mathrm{II}}^{\mathrm{tip}}}{K_{\mathrm{II}}} = 1+\frac{wl}{4\pi r_0(r_0+l)}\left(C_6+C_1+\frac{9}{4}C_2\right)-\frac{E_{\mathrm{m}}w}{\sqrt{2\pi}K_{\mathrm{II}}}C_5e_{12}^{T*}\left(\frac{1}{\sqrt{r_0+l}}-\frac{1}{\sqrt{r_0}}\right). \tag{28}$$

4 Numerical examples and discussion

As an example, Fig. 3 shows the variations of the normalized configuration force (CF) and crack tip stress intensity factor (SIF) for a pair of isosceles right-angled triangular inclusions which are symmetrically about the crack line at different angles θ for various stress-free transformation strains $\mathbf{e}^{\mathrm{T}*}$. When the effect of stress-free transformation strain is considered, the normalized repulsion force ($F_r > 0$) decreases for $\alpha > 1$, and

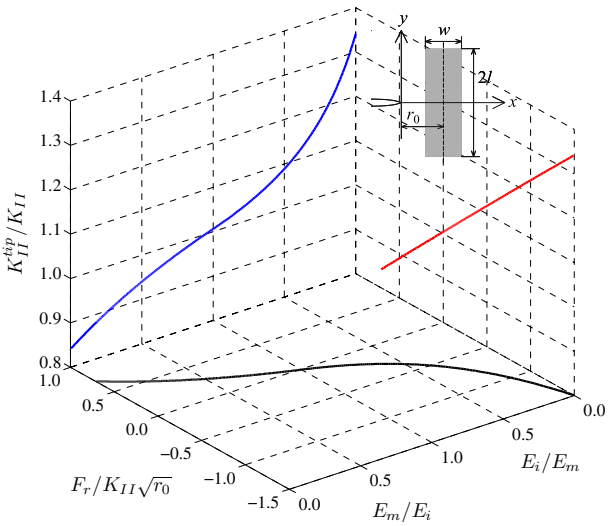

Fig. 4 Normalized $CFF_r/K_{\mathrm{II}}\sqrt{r_0}$ and SIF$K_{\mathrm{II}}^{\mathrm{tip}}/K_{\mathrm{II}}$ as functions of E_i/E_m for a mode II crack interacting with a rectangular inclusion of $e_{11}^{T*} = e_{22}^{T*} = 0.02$, $e_{12}^{T*} = 0.04$ calculated from Eqs. (13) and (18), respectively, at the fixed $r_0 = w = l/1.5$, $\nu = 0.3$, and $K_{\mathrm{II}}/E_{\mathrm{m}}\sqrt{r_0} = 1$

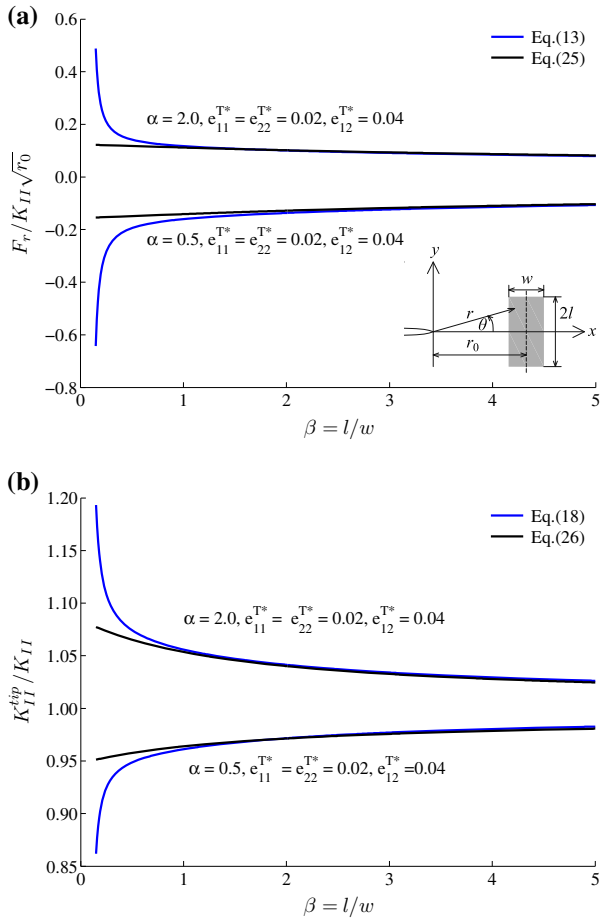

Fig. 5 Normalized CF$F_r/K_{\mathrm{II}}\sqrt{r_0}$ and SIF$K_{\mathrm{II}}^{\mathrm{tip}}/K_{\mathrm{II}}$ as functions of β for a mode II crack interacting with a rectangular inclusion of $\alpha = 0.5, 2.0$ and $e_{11}^{T*} = e_{22}^{T*} = 0.02$, $e_{12}^{T*} = 0.04$ at the fixed $\nu = 0.3$ and $K_{\mathrm{II}}/E_{\mathrm{m}}\sqrt{r_0} = 1$

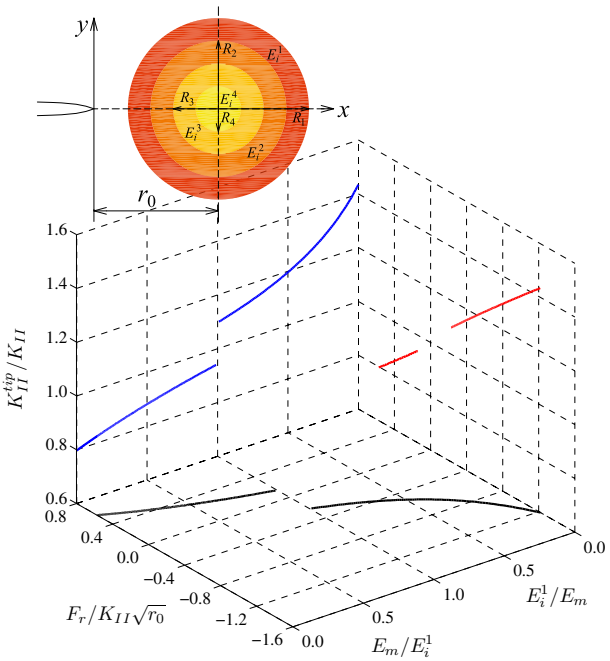

Fig. 6 Normalized CF$F_r/K_{\rm II}\sqrt{r_0}$ and SIF$K_{\rm II}^{\rm tip}/K_{\rm II}$ as functions of $E_{\rm i}^1/E_{\rm m}$ for a mode II crack interacting with a multilayer circular inclusion of $e_{11}^{T*} = e_{22}^{T*} = 0.02$, $e_{12}^{T*} = 0.04$ calculated from Eqs. (13) and (18), respectively, at the fixed $r_0 : R_1 : R_2 : R_3 : R_4 = 1.5 : 1.0 : 0.75 : 0.5 : 0.25$, $\nu = 0.3$ and $K_{\rm II}/E_{\rm m}\sqrt{r_0} = 1$

the attraction force ($F_r < 0$) increases for $\alpha < 1$. On the other hand, the normalized stress intensity factor increases for both $\alpha > 1$ and $\alpha < 1$.

Figure 4 shows a relationship between the E_i/E_m, the normalized CF and SIF. The CF between the mode II crack and a rectangular inclusion is attraction for a soft one ($E_i/E_m < 1$) and repulsion for a hard inclusion ($E_i/E_m > 1$), which is in accordance with the prediction that a soft (hard) inclusion enhances (reduces) the effective SIF. When $E_i/E_m < 1$, the normalized attraction force increases as the modulus ratio decreases and the normalized SIF also increases as the modulus ratio decreases, indicating that the conditions are more favorable for the crack penetration. When $E_i/E_m > 1$, the normalized repulsion force increases as the modulus ratio increases, and the normalized SIF decreases as the modulus ratio increases, suggesting that the conditions accelerate the crack deflection.

To check the accuracy of the approximate solution, the interaction of a crack and a rectangular inclusion of area $w \times 2l = r_0^2$ centered at $(r_0, 0)$ where r_0 is a constant is shown in Fig. 5. The normalized CF$F_r/K_{\rm II}\sqrt{r_0}$ and SIF$K_{\rm II}^{\rm tip}/K_{\rm II}$ as functions of $\beta(= l/w)$ for $\alpha = 0.5, 2$ are obtained by integrating Eqs. (13) and (18), respectively, under the condition that the rectangular inclusion keeps its area constant, but changes its shape. The approximate values of Eqs. (25) and (26) are compared with the integrating values of Eqs. (13) and (18) for the case of $\beta = l/w >> 1$, respectively. As shown in Fig. 5, the approximate Eqs. (25) and (26) for $\beta > 1.5$ agree well with the prediction of Eqs. (13) and (18), respectively.

Figure 6 shows the mode II crack interacting with the multi-phase elastic inclusion centered at $(r_0, 0)$, which is a four-layer circular inclusion with different modulus. The elastic modulus for the soft inclusion and hard inclusion is $E_{\rm i}^{j+1} = 0.5E_{\rm i}^j$ and $E_{\rm i}^{j+1} = 2E_{\rm i}^j (j = 1, 2, 3)$, respectively. As shown in Fig. 6, it suggests that the CF between a mode II crack and the multi-phase inclusion is attraction for a soft one and repulsion for a hard inclusion, which is in agreement with the prediction that a soft (hard) inclusion ahead of a mode II crack enhances (reduces) the effective SIF for the modulus ratio ($0 \sim \infty$) between the matrix and the multi-phase inclusion.

In the engineering applications, the interaction between a crack and inclusion behaves in three dimensions (3D). However, it is difficult to find an analytical solution for the three-dimensional problem, and an alternative approach is to simplify the 3D problem into 2D. On the other hand, the plane strain and plane stress describe two typical cases of the triaxial stress state. As shown in Fig. 7, for both CF and SIF, the predictions of the plane stress solution fairly approach to the plane strain for most engineering materials with a Poisson's ratio

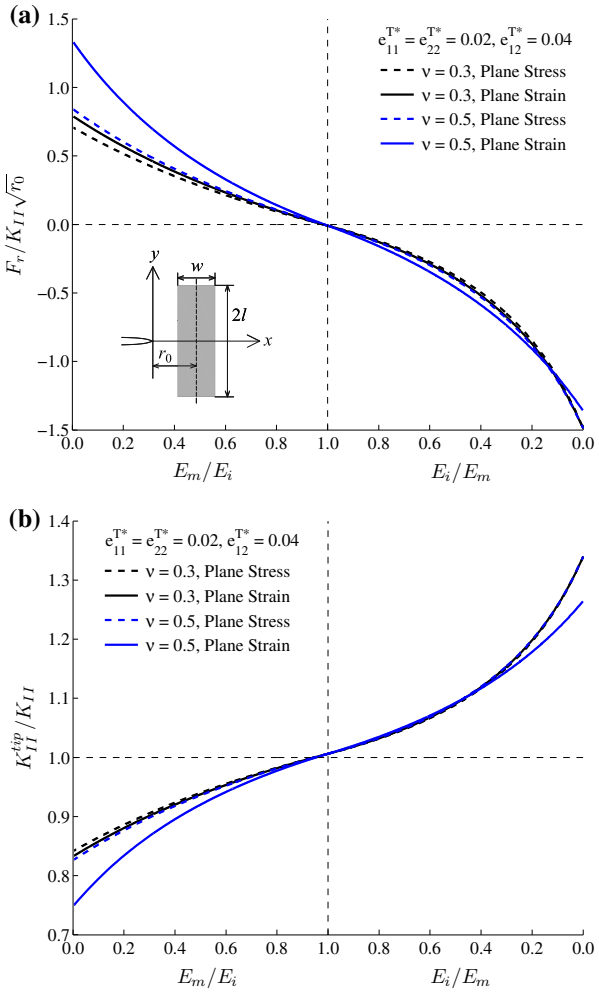

Fig. 7 Normalized CF $F_r/K_{\mathrm{II}}\sqrt{r_0}$ and SIF $K_{\mathrm{II}}^{\mathrm{tip}}/K_{\mathrm{II}}$ as functions of E_i/E_m for a mode II crack interacting with a rectangular inclusion of $e_{11}^{T*} = e_{22}^{T*} = 0.02$, $e_{12}^{T*} = 0.04$ calculated from Eqs. (13) and (18) for plane stress and plane strain, respectively, at the fixed $r_0 = w = l/1.5$, $\nu = 0.3$, $\nu = 0.5$ and $K_{\mathrm{II}}/E_{\mathrm{m}}\sqrt{r_0} = 1$

$\upsilon = 0.3$. The prominent difference between plane stress and plane strain occurs only at a large υ-value (e.g., $\upsilon = 0.5$). Hence, it is expected that the 2D solution may approach the 3D analysis.

Finally, it should be noted that the Eshelby equivalent inclusion theory is mathematically rigorous only for an infinite matrix containing a single ellipsoidal inclusion. But many activities have been made to extend it into different problems for using the Eshelby theory in more engineering problems [26–29]. As validated by experimental results [30], some numerical examples [8,15,16] and available classical solutions [31], the extended application of the Eshelby theory has extremely good accuracy.

5 Conclusions

Based on the Eshelby theory, an inhomogeneous inclusion can be transformed into a homogenous one with an equivalent transformation strain. The interaction between crack and inclusion can then be evaluated from the configuration force theory and transformation toughening theory. General solutions for the stress intensity factor (SIF) and configuration force (CF) to investigate the interaction between a plane stress mode II crack and an inhomogeneous inclusion of arbitrary shape undergoing some stress-free transformation strain are developed, respectively, and some simplified approximate solutions for several special inclusion shapes are obtained which are very beneficial for engineering applications. The present solutions provide a novel method to interpret the behavior of crack penetration/deflection in the composite films. It is worth to note that the

special advantage of the present approach is that the basic equation, in an integral form, can be customarily used to the inclusion with arbitrary shape.

Acknowledgements The authors would like to acknowledge the financial support by the National Natural Science Foundation of China (No. 51175404).

References

1. Ubale, A.U., Deshpande, V.P.: Effect of manganese inclusion on structural, optical and electrical properties of ZnO thin films. J. Alloy Compd. **500**, 138–143 (2010)
2. Park, S., Ji, H.Y., Kim, M.J., Peck, J.H., Kim, K.: Enhanced quantum efficiency of amorphous silicon thin film solar cells with the inclusion of a rear-reflector thin film. Appl. Phys. Lett. **104**, 073902 (2014)
3. Pappacena, K.E., Singh, D., Ajayi, O.O., Routbort, J.L., Erilymaz, O.L., Demas, N.G., Chen, G.: Residual stresses, interfacial adhesion and tribological properties of MoN/Cu composite coatings. Wear **278**, 62–70 (2012)
4. Liu, M., Wang, X., Liu, Q., Gao, H.: Application of smart coating sensor in crack detection for aircraft. Appl. Mech. Mater. **152–154**, 554–559 (2012)
5. Sun, Y., Liu, M.: Analysis of the crack penetration/deflection at the interfaces in the intelligent coating system utilizing virtual crack closure technique. Eng. Fract. Mech. **133**, 152–162 (2015)
6. Freund, L., Suresh, S.: Thin Film Materials: Stress, Defect Formation and Surface Evolution. Cambridge University Press, Cambridge (2003)
7. Steffensen, S., Kibsgaard, R.L., Jensen, H.M.: Debonding of particles in thin films. Int. J. Solid Struct. **51**, 2850–2856 (2014)
8. Sun, Y., Yang, J., Wang, B., Liu, M.: The interaction of the plane stress mode I crack with an inhomogeneity undergoing a stress-free transformation strain. Int. J. Appl. Mech. **7**, 1550040 (2015)
9. Zhou, K., Hoh, H.J., Wang, X., Keer, L.M., Pang, J.H., Song, B., Wang, Q.J.: A review of recent works on inclusions. Mech. Mater. **60**, 144–158 (2013)
10. Taya, M., Chou, T.W.: On two kinds of ellipsoidal inhomogeneities in an infinite elastic body: an application to a hybrid composite. Int. J. Solid Struct. **17**, 553–563 (1981)
11. Wang, X., Pan, E., Chung, P.W.: On a semi-infinite crack penetrating a piezoelectric circular inhomogeneity with a viscous interface. Int. J. Solid Struct. **46**, 203–216 (2009)
12. Eshelby, J.D.: The determination of the elastic fields of an ellipsoidal inclusion and related problems. Proc. R. Soc. Lond. Ser. A **241**, 376–396 (1957)
13. Lambropoulos, J.C.: Shear, shape and orientation effects in transformation toughening. Int. J. Solid Struct. **22**, 1083–1106 (1986)
14. Eshelby, J.D.: The force on an elastic singularity. Philos. Trans. R. Soc. Lond. Ser. A **244**, 87–112 (1951)
15. Li, Z., Chen, Q.: Crack-inclusion interaction for mode I crack analyzed by Eshelby equivalent inclusion method. Int. J. Fract. **118**, 29–40 (2002)
16. Yang, L., Chen, Q., Li, Z.: Crack-inclusion interaction for mode II crack analyzed by Eshelby equivalent inclusion method. Eng. Fract. Mech. **71**, 1421–1433 (2004)
17. Li, H., Yang, J., Li, Z.: An approximate solution for the plane stress mode I crack interacting with an inclusion of arbitrary shape. Eng. Fract. Mech. **116**, 190–196 (2014)
18. Yang, J., Li, H., Li, Z.: Approximate analytical solution for plane stress mode II crack interacting with an inclusion of any shape. Eur. J. Mech. A/Solid **49**, 293–298 (2015)
19. Zhou, R., Li, Z., Sun, J.: Crack deflection and interface debonding in composite materials elucidated by the configuration force theory. Compos Part B **42**, 1999–2003 (2011)
20. Brencich, A., Carpinteri, A.: Stress field interaction and strain energy distribution between a stationary main crack and its process zone. Eng. Fract. Mech. **59**, 797–814 (1998)
21. Withers, P.J., Stobbs, W.M., Pedersen, O.B.: The application of the Eshelby method of internal stress determination to short fibre metal matrix composites. Acta Metall. **37**, 3061–3084 (1989)
22. Li, Z., Yang, L.: The application of the Eshelby equivalent inclusion method for unifying modulus and transformation toughening. Int. J. Solid Struct. **39**, 5225–5240 (2002)
23. Mura, T.: Micromechanics of Defects in Solids, 2nd edn. Martinus Nijhoff Publishers, Dordrecht (1987)
24. Mura, T.: A theory of fatigue crack initiation. Mater. Sci. Eng. A **176**, 61–70 (1994)
25. Gross, D., Mueller, R., Kolling, S.: Configurational forces-morphology evolution and finite elements. Mech. Res. Commun. **29**, 529–536 (2002)
26. Sharma, P., Ganti, S.: Size-dependent Eshelby's tensor for embedded nano-inclusions incorporating surface/interface energies. J. Appl. Mech. **71**, 663–671 (2004)
27. Zhou, K., Keer, L.M., Wang, Q.J., Ai, X.L., Sawamiphakdi, K., Glaws, P., Paire, M., Che, F.: Interaction of multiple inhomogeneous inclusions beneath a surface. Comput. Method. Appl. Mech. Eng. **217**, 25–33 (2012)
28. Wang, X., Zhou, K.: Long-range interaction of a line dislocation with multiple multicoated inclusions of arbitrary shape. Acta Mech. **224**, 63–70 (2013)
29. Chen, Q.D., Xu, K.Y., Pan, E.: Inclusion of an arbitrary polygon with graded eigenstrain in an anisotropic piezoelectric half plane. Int. J. Solid Struct. **51**, 53–62 (2014)
30. Ippolito, M., Mattoni, A., Colombo, L., Pugno, N.: Role of lattice discreteness on brittle fracture: atomistic simulations versus analytical models. Phys. Rev. B **73**, 104111 (2006)
31. Shi, J., Li, Z.: The interaction of an edge dislocation with an inclusion of arbitrary shape analyzed by the Eshelby inclusion method. Acta Mech. **161**, 31–37 (2003)